Evolution of the early Antarctic ice ages

Diederik Liebrand[a,1], Anouk T. M. de Bakker[b,c], Helen M. Beddow[d], Paul A. Wilson[a], Steven M. Bohaty[a], Gerben Ruessink[b], Heiko Pälike[e], Sietske J. Batenburg[f,g], Frederik J. Hilgen[d], David A. Hodell[h], Claire E. Huck[a], Dick Kroon[i], Isabella Raffi[j], Mischa J. M. Saes[d], Arnold E. van Dijk[d], and Lucas J. Lourens[d]

[a]National Oceanography Centre Southampton, University of Southampton, Southampton SO14 3ZH, United Kingdom; [b]Department of Physical Geography, Faculty of Geosciences, Utrecht University, 3508 TC Utrecht, The Netherlands; [c]Littoral Environnement et Sociétés, Université de La Rochelle, 17042 La Rochelle, France; [d]Department of Earth Sciences, Faculty of Geosciences, Utrecht University, 3584 CD Utrecht, The Netherlands; [e]Center for Marine Environmental Sciences, University of Bremen, 28359 Bremen, Germany; [f]Institute of Geosciences, Goethe-University Frankfurt am Main, 60438 Frankfurt, Germany; [g]Department of Earth Sciences, University of Oxford, Oxford OX1 3AN, United Kingdom; [h]Department of Earth Sciences, University of Cambridge, Cambridge CB2 3EQ, United Kingdom; [i]School of GeoSciences, Grant Institute, University of Edinburgh, Edinburgh EH9 3FE, United Kingdom; and [j]Dipartimento di Ingegneria e Geologia, Università degli Studi "G. d'Annunzio" di Chieti–Pescara, 66013 Chieti Scalo, Italy

Edited by Mark H. Thiemens, University of California, San Diego, La Jolla, CA, and approved February 24, 2017 (received for review September 15, 2016)

Understanding the stability of the early Antarctic ice cap in the geological past is of societal interest because present-day atmospheric CO_2 concentrations have reached values comparable to those estimated for the Oligocene and the Early Miocene epochs. Here we analyze a new high-resolution deep-sea oxygen isotope ($\delta^{18}O$) record from the South Atlantic Ocean spanning an interval between 30.1 My and 17.1 My ago. The record displays major oscillations in deep-sea temperature and Antarctic ice volume in response to the ~110-ky eccentricity modulation of precession. Conservative minimum ice volume estimates show that waxing and waning of at least ~85 to 110% of the volume of the present East Antarctic Ice Sheet is required to explain many of the ~110-ky cycles. Antarctic ice sheets were typically largest during repeated glacial cycles of the mid-Oligocene (~28.0 My to ~26.3 My ago) and across the Oligocene–Miocene Transition (~23.0 My ago). However, the high-amplitude glacial–interglacial cycles of the mid-Oligocene are highly symmetrical, indicating a more direct response to eccentricity modulation of precession than their Early Miocene counterparts, which are distinctly asymmetrical—indicative of prolonged ice buildup and delayed, but rapid, glacial terminations. We hypothesize that the long-term transition to a warmer climate state with sawtooth-shaped glacial cycles in the Early Miocene was brought about by subsidence and glacial erosion in West Antarctica during the Late Oligocene and/or a change in the variability of atmospheric CO_2 levels on astronomical time scales that is not yet captured in existing proxy reconstructions.

unipolar icehouse | early Antarctic ice sheet | Oligocene–Miocene | glacial–interglacial cycle geometries | bispectral analysis

The early icehouse world of the Oligocene and Early Miocene epochs (hereafter referred to as Oligo-Miocene) is bracketed by two major climate events: the Eocene–Oligocene Climate Transition (~34 My ago, EOT) and the onset of the Middle Miocene Climatic Optimum (~17 My ago) (1). Deep-sea proxy records and sedimentological evidence from the Antarctic continental shelves indicate the expansion of continental-size ice sheets on Antarctica at the EOT (2, 3), and sedimentary records from the western Ross Sea on the East Antarctic margin document large subsequent oscillations in ice sheet extent on astronomical time scales during the Oligo-Miocene (4). In contrast, large ice sheets did not develop in the high northern latitudes until the Late Pliocene (5). Thus, the Oligo-Miocene presents an opportunity to study the dynamics of a unipolar (Antarctic) icehouse climate state without the overprint of Northern Hemisphere ice sheets on benthic foraminiferal $\delta^{18}O$ records. Published proxy records of atmospheric CO_2 concentration show a decline from the Oligocene to the Miocene (6, 7) that is broadly contemporaneous with a strong minimum in the ~2.4-My eccentricity cycle ~24 My ago (8), which would promote continental ice sheet expansion if radiative forcing was the dominant control on ice volume. Previous studies using drill core records from the deep ocean demonstrate a climatic response to astronomical forcing for the Oligocene (9, 10) and parts of the Miocene (11–13). However, to improve understanding of the behavior of the climate/cryosphere system, we need longer high-resolution records from strategic locations that capture the changing response of the high latitudes to the combined effects of CO_2, astronomical forcing, and tectonic boundary conditions.

Walvis Ridge Ocean Drilling Program Site 1264

To shed light on southern high-latitude climate variability through the Oligo-Miocene, we analyze a new high-resolution benthic foraminiferal $\delta^{18}O$ record from Walvis Ridge, located in the southeastern Atlantic Ocean [Ocean Drilling Program Site 1264; 2,505-m water depth; 2,000- to 2,200-m paleowater depth; 28.53°S, 2.85°E, Fig. 1 (14, 15)]. An astrochronology for Site 1264 was developed by tuning $CaCO_3$ estimates to the stable eccentricity solution independently of the benthic $\delta^{18}O$ record (15). On the eccentricity-tuned age model, the Site 1264 record spans a 13-My time window between 30.1 My and 17.1 My ago and ranges between 405-ky Eccentricity Cycles 74 to 43 and ~2.4-My Eccentricity Cycles 13 to 8 (Fig. 1) (15), representing the first continuous record from a single site spanning the mid-Oligocene to Early Miocene. Five distinct time intervals with clear multimillion-year climatic trends are identified in this new $\delta^{18}O$ dataset from Walvis Ridge: (*i*) an Early Oligocene time interval of climate deterioration (~30.1 My to 28.0 My ago); (*ii*)

Significance

The Antarctic ice cap waxed and waned on astronomical time scales throughout the Oligo-Miocene time interval. We quantify geometries of Antarctic ice age cycles, as expressed in a new climate record from the South Atlantic Ocean, to track changing dynamics of the unipolar icehouse climate state. We document numerous ~110-thousand-year-long oscillations between a near-fully glaciated and deglaciated Antarctica that transitioned from being symmetric in the Oligocene to asymmetric in the Miocene. We infer that distinctly asymmetric ice age cycles are not unique to the Late Pleistocene or to extremely large continental ice sheets. The patterns of long-term change in Antarctic climate interpreted from this record are not readily reconciled with existing CO_2 records.

Author contributions: D.L., A.T.M.d.B., H.M.B., P.A.W., S.M.B., G.R., H.P., S.J.B., F.J.H., D.A.H., C.E.H., D.K., I.R., M.J.M.S., A.E.v.D., and L.J.L. designed research; D.L., A.T.M.d.B., H.M.B., M.J.M.S., and A.E.v.D. performed research; P.A.W., G.R., H.P., F.J.H., and L.J.L. contributed analytic tools; D.L., A.T.M.d.B., H.M.B., M.J.M.S., and A.E.v.D. analyzed data; D.L., A.T.M.d.B., P.A.W., and S.M.B. wrote the paper; and all other authors contributed to writing the paper.

The authors declare no conflict of interest.

This article is a PNAS Direct Submission.

Freely available online through the PNAS open access option.

[1]To whom correspondence should be addressed. Email: diederik.liebrand@noc.soton.ac.uk.

This article contains supporting information online at www.pnas.org/lookup/suppl/doi:10.1073/pnas.1615440114/-/DCSupplemental.

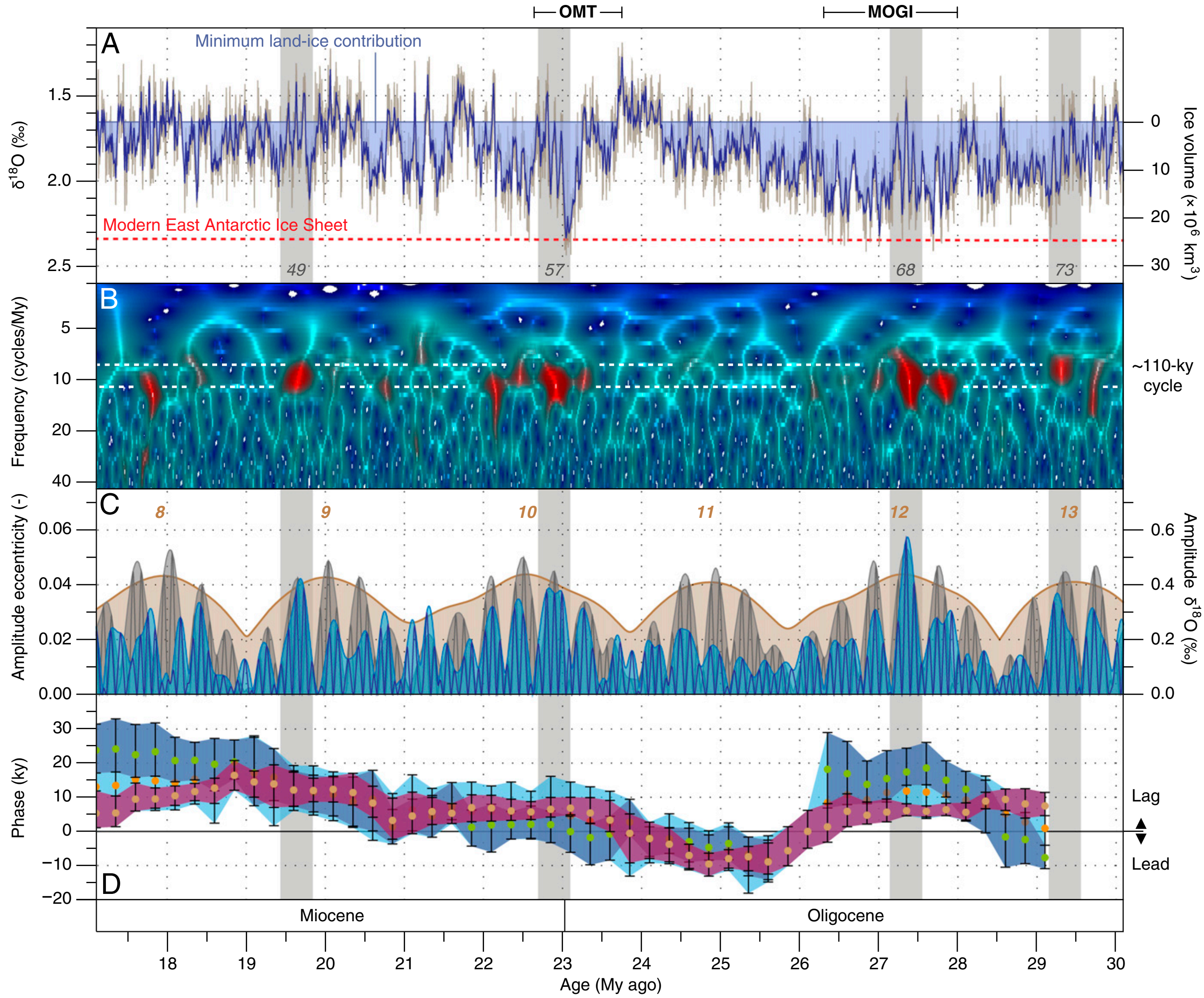

Fig. 1. High-latitude climate–cryosphere evolution during the Oligo-Miocene and sinusoidal glacial–interglacial cycle properties. (*A*) Benthic foraminiferal (*Cibicides mundulus*) $\delta^{18}O$ record from ODP Site 1264 (gray line) (15) and SiZer smooth (blue line; see *SI Methods*). Minimum ice volume contribution (lilac area, right axis) to the benthic $\delta^{18}O$ record is calculated relative to all values exceeding 1.65‰ (left axis; see *SI Methods*). Dashed red line represents the contribution to benthic $\delta^{18}O$ of a present-day-sized East Antarctic Ice Sheet ($\delta^{18}O_{ice}$ = –42‰). (*B*–*D*) Sinusoidal glacial–interglacial cycle properties. (*B*) Wavelet analysis of the Site 1264 benthic $\delta^{18}O$ record. White dashed lines represent the ~95- and ~125-ky eccentricity periodicities. (*C*) Filter of the Site 1264 benthic $\delta^{18}O$ record centered around the ~110-ky periodicity (dark blue line) and its amplitude modulation (light blue line and area), compared with those of eccentricity (gray lines and area). The filter values are proportional to the eccentricity (left axis) and the VPDB (Vienna Pee Dee Belemnite) scale (right axis). In the background (light brown line and area), the ~2.4-My component of Earth's orbital eccentricity is shown (+0.02 to aid visibility) and marked by brown bold italic cycle numbers. (*D*) Phase evolution of the ~125-ky (dark blue area, green dots), ~95-ky (purple area, brown dots), and combined (including intermediate frequencies) ~110-ky (light blue area, orange dots) cycles to eccentricity, which are independant from one other. Vertical gray bars represent 405-ky Eccentricity Cycles 49, 57, 68, and 73 (dark gray italic numbers), characterized by exceptionally strong ~110-ky responses in benthic $\delta^{18}O$ (Fig. 3 *B*–*E*) (15).

a generally cold but highly unstable mid-Oligocene time interval (~28.0 My to 26.3 My ago), which we refer to as the Mid-Oligocene Glacial Interval (MOGI); (*iii*) a Late Oligocene time interval characterized by low-amplitude climate variability and stepwise climatic amelioration (~26.3 My to 23.7 My ago), confirming that this warming trend is a real feature of Cenozoic climate history (9) rather than an artifact of composite records from multiple sites in different ocean basins; (*iv*) a time interval of persistently high-amplitude climate variability spanning the Oligocene–Miocene Transition (OMT) and the earliest Miocene (~23.7 My to 20.4 My ago); and (*v*) a time interval of moderate-amplitude climate variability during the latter part of the Early Miocene (~20.4 My to 17.1 My ago).

Following the MOGI, the Late Oligocene warming phase proceeded in a series of three distinct steps (~26.3, ~25.5, and ~24.2 My ago), with the peak warming/lowest ice volume confined to a ~500-ky period (~24.2 My to 23.7 My ago). This climate state was terminated by the OMT (~23.7 My to 22.7 My ago), which consists of two rapid ~0.5‰ increases in benthic $\delta^{18}O$ that are separated by an interval (405-ky eccentricity cycle long) of partial $\delta^{18}O$ recovery (15). The onset of the OMT is thereby comparable in structure to the EOT (3). A 405-ky-long overall decrease in benthic $\delta^{18}O$ marks the recovery phase of the OMT.

Ice Volume Estimates

To better understand the significance of the documented $\delta^{18}O$ variability on long-term change in the high-latitude climate system, we make a conservative estimate of the minimum contribution of continental ice volume to the Site 1264 benthic $\delta^{18}O$ signal by assuming that Oligo-Miocene bottom-water temperatures at Site 1264 were never colder than the current temperature of 2.5 °C and applying an average $\delta^{18}O$ composition of Oligo-Miocene ice sheets ($\delta^{18}O_{ice}$) of −42‰ Vienna standard mean ocean water (VSMOW) (*SI Methods*) (16). These minimum ice volume estimates (Fig. 1) do not fully account for the changing relative contributions of ice volume and deep-sea temperature to the benthic $\delta^{18}O$ signal over glacial–interglacial cycles. However, they are largely consistent with estimates of glacioeustatic sea level change from the New Jersey shelf (17) and those generated by inverse models of (multisite composite) $\delta^{18}O$ records (12, 18). These ice volume estimates and sea level reconstructions strongly suggest that a very large part of the benthic $\delta^{18}O$ signal is linked to large ice volume changes on Antarctica.

Three major results stand out in the minimum ice volume calculations on the Site 1264 benthic $\delta^{18}O$ record (Fig. 1*A*). First, excluding the OMT interval, the Oligocene glacials are characterized by larger continental ice sheet volumes than those of the Early Miocene, particularly during the MOGI. Second, across the OMT, Antarctica transitioned from a climate state that was near-fully deglaciated to one characterized by an ice sheet as large as the present East Antarctic Ice Sheet and back into a near-fully deglaciated state in less than 1 My. Third, many glacial–interglacial cycles in the benthic $\delta^{18}O$ record are associated with a $\delta^{18}O_{sw}$ change of at least ∼0.60 to 0.75‰, requiring the waxing and waning of $\sim 21–26 \times 10^6$ km^3 of ice, or ∼85 to 110% of present East Antarctic ice volume, on timescales of ≤110 ky.

Sinusoidal Glacial–Interglacial Cycle Properties

The 13 My-long Oligo-Miocene benthic $\delta^{18}O$ record from Site 1264 shows distinct cyclicity on astronomical time scales. Wavelet analysis reveals (Fig. 1 and Fig. S1) (15) that the amplitude of variability at the ∼110-ky eccentricity periodicity is particularly pronounced (≥1.0‰ across the larger $\delta^{18}O$ cycles). The amplitude of the 40-ky obliquity periodicity is subdued in comparison with published records from other sites, presumably because of the higher sedimentation rates at those sites (13, 19). Four relatively short (405 ky long) intervals with particularly strong ∼110-ky-paced $\delta^{18}O$ variability are also identified in the record (vertical gray bars, Fig. 1), demonstrating a pronounced climate–cryosphere response to eccentricity-modulated precession of Earth's spin axis (15). These intervals are contemporaneous with 405-ky eccentricity maxima during ∼2.4-My eccentricity maxima, specifically 405-ky Cycles 73, 68, 57, and 49. Thus, although the OMT deserves its status as a major transient Cenozoic event (1, 20) because it is a prominent but transient glacial episode that abruptly terminates Late Oligocene warming, the amplitude of ice age cycles observed as the climate system emerges from peak glacial OMT conditions is not unique in the Oligo-Miocene. In fact, this recovery phase of the OMT is one of four Oligo-Miocene intervals characterized by particularly high-amplitude ∼110-ky oscillations between glacial and interglacial Antarctic conditions (Fig. 1*A*). The record from Site 1264 is the first to unequivocally show that the ∼2.4-My eccentricity cycle paces recurrent episodes of high-amplitude ∼110-ky variability in benthic $\delta^{18}O$ (9, 19) and provides a new global climatic context in which to understand Oligo-Miocene glacial history, carbon cycling (9, 21), midlatitude terrestrial water balance (22), and mammal turnover rates (23) that show similar pacing. The intervals with particularly strong ∼110-ky cycles are separated by prolonged periods of attenuated ∼110-ky cycle amplitude, indicating that not all ∼2.4-My and 405-ky eccentricity maxima trigger similar cryospheric responses (Fig. 1). Specifically, ∼2.4-My Eccentricity Cycle 11 in the Late Oligocene is not characterized by high-amplitude ∼110-ky cycles (Fig. 1). Furthermore, no consistent relationship is found between strong ∼110-ky cycles in benthic $\delta^{18}O$ and the ∼1.2-My amplitude modulation of obliquity (15). This inconsistency suggests that some other factor or combination of factors is responsible for the changing response of the climate system to astronomical forcing on ∼110-ky time scales over the Oligo-Miocene.

We assess the phase relationships of the tuned $\delta^{18}O$ data with respect to the main frequencies of orbital eccentricity to track the response times of the Oligo-Miocene climate system (Fig. 1 and Figs. S2 and S3). The benthic $\delta^{18}O$ record from Site 1264 displays a marked multimillion-year evolution in the phasing of the ∼110-ky cycle relative to eccentricity, starting with a ∼10-ky phase lag during the mid-Oligocene, followed by an unstable phase relation at ∼26 My ago and a steady increase in phase that culminates in a 10- to 15-ky lag at ∼19.0 My ago (Fig. S3). The ∼95- and ∼125-ky frequencies show largely independent phase evolutions. On the basis of these data alone, we cannot rule out the possibility that part of the observed structure in the long-term phase evolution arises from changes in the proportional contribution of temperature and ice volume to benthic $\delta^{18}O$ (24). However, the observed changes in phase are so large (approximately −10 ky to +15 ky) that changes in the response time of Antarctic ice sheets are most likely responsible; large continental ice sheets are the slowest-responding physical component of Earth's climate system and the only mechanism capable of inducing phase lags in deep-sea benthic $\delta^{18}O$ records of ∼10 ky to 15 ky (25). Analysis of phasing suggests that, over full glacial–interglacial cycles, the high-latitude climate–Antarctic ice sheet system responded more slowly to astronomical pacing during the MOGI (∼28.0 My to 26.3 My ago) and Early Miocene ($\lesssim$23 My ago) than during either the Early Oligocene (∼30.1 My to 28.0 My ago) or Late Oligocene (∼26.3 My to 23.7 My ago).

Bispectral Analysis

To investigate phase coupling between (astronomical) cycles embedded in the Site 1264 benthic $\delta^{18}O$ record, we apply bispectral techniques (26–28). A bispectrum identifies phase couplings between three frequencies: f_1, f_2, and their sum frequency $f_1 + f_2 = f_3$. When phase-coupled, energy transfers nonlinearly between these frequencies and is redistributed over the spectrum. This transfer of spectral energy results in lower and higher harmonics and in the formation of skewed and/or asymmetric cycle geometries such as those observed in the $\delta^{18}O$ record. We compare bispectra for two selected time intervals with strong ∼110-ky cyclicity (Fig. 2): a mid-Oligocene interval (including the MOGI), during ∼2.4-My Eccentricity Cycle 12 (28.30 My to 26.30 My ago), and an OMT-spanning interval, during ∼2.4-My Eccentricity Cycle 10 (23.54 My to 21.54 My ago). A third, Early Miocene example is considered in Fig. S4. The bispectra show that, during both the MOGI and the OMT, numerous phase couplings occur with frequencies that include, but are not limited to, astronomical cycles. Most interactions occur between cycles with periodicities close to those of eccentricity (periods of 405, ∼125, and ∼95 ky per cycle, equal to frequencies of 2.5, 8.0, and 10.5 cycles per million years, respectively) that exchange energy among themselves and also with higher frequencies. The close proximity of both positive and negative interactions around eccentricity frequencies (Fig. 2 and Fig. S4) suggests that these frequencies redistribute energy by broadening spectral peaks in $\delta^{18}O$. This process may explain the observed ∼200-ky cycle (15). The main difference between the two selected time intervals is that the OMT bispectrum reveals many more nonlinear interactions (Fig. 2), both positive and negative, which indicates that the climate–cryosphere system responded in a more complex and indirect manner to insolation forcing across the OMT than during the MOGI. This observation may point to the activation of heightened positive feedback mechanisms across the OMT related to continental ice sheet growth and decay (13, 29), possibly involving the carbon cycle (30) or Antarctic sea ice (31).

Nonsinusoidal Glacial–Interglacial Cycle Properties

To further understand the nonlinearity in the climate system documented by the bispectra, we assess nonsinusoidal (i.e., non-Gaussian) cycle properties (Fig. 3 and Figs. S5–S8; see also *SI Exploring Potential Cycle Shape Distortion*). Nonlinearity in climate cycles can be quantified in terms of skewness, asymmetry, and kurtosis using standard and higher-order spectral analyses to elucidate

EARTH, ATMOSPHERIC, AND PLANETARY SCIENCES

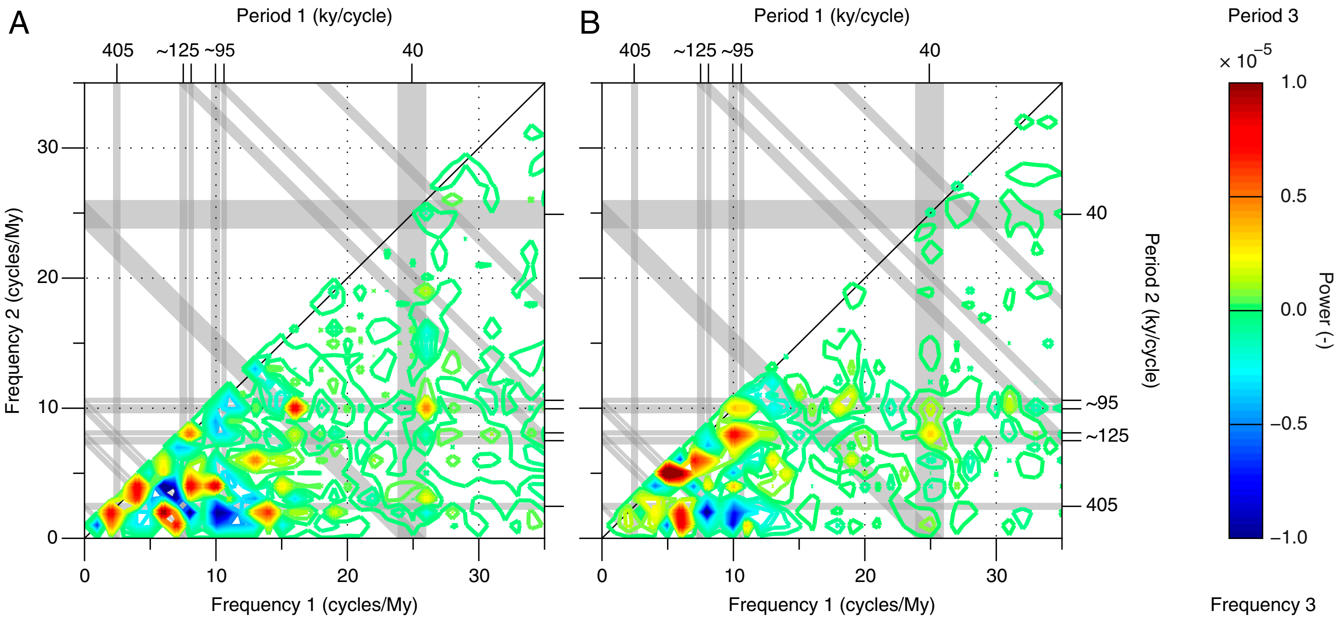

Fig. 2. Bispectra assessing phase coupling and energy transfers between frequencies in the $\delta^{18}O$ data. Bispectral analyses on benthic $\delta^{18}O$ across two, 2-My-long windows with strong ~110-ky cycles (see also Fig. S4). (*A*) Bispectrum across the OMT interval, during ~2.4-My Eccentricity Cycle 10 (23.54 My to 21.54 My ago). (*B*) Bispectrum across the MOGI, during ~2.4-My Eccentricity Cycle 12 (28.30 My to 26.30 My ago). The colors of the bispectrum show the direction of the energy transfers. The intensity of the colors is indicative of the magnitude of energy transfers (see *SI Methods*). Red indicates a transfer of spectral power from two frequencies, f_1 (see *x* axes) and f_2 (see *y* axes), to frequency f_3 ($f_1 + f_2 = f_3$). In contrast, blue represents a gain of spectral power at frequencies f_1 and f_2 from frequency f_3. Gray lines reflect the main astronomical frequencies of eccentricity, obliquity, and precession.

the rapidity of climatic transitions (see *SI Methods*). The remarkably consistent negative skewness in the $\delta^{18}O$ record (mean −0.18; Fig. 3 and Fig. S8) indicates that Oligo-Miocene glacials were longer in duration than interglacials—a result that is consistent with the Late Pleistocene record (Fig. S5) (27, 28, 32). To assess the time spent per cycle in full glacial and full interglacial conditions (in contrast to skewness which records the duration of glacials versus interglacials), we also calculate the evolution of cycle kurtosis through the benthic $\delta^{18}O$ record. Square-waved (platykurtic) glacial–interglacial cycles are more evident in the Site 1264 record than thin-peaked (leptokurtic) ones, apart from an Early Miocene interval between ~21.5 My and 19.0 My ago when leptokurtic cycles prevail (Fig. 3 and Fig. S8). This observation indicates that the Oligo-Miocene climate system generally favored full glacial and full interglacial conditions and transitioned rapidly between those two climate states. We attribute this finding to the operation of well-documented strong positive feedbacks on ice sheet growth and decay (25, 29).

To understand the relative rates of ice sheet growth versus decay, we quantify cycle asymmetry. Although the Site 1264 record shows consistently skewed Oligo-Miocene ~110-ky glacial–interglacial cycles, we document a major change over time in the symmetry of those cycles that is marked by a transition to more asymmetric cycles that began ~23 My ago at the OMT. This change represents a shift to a new climatic state characterized by a ~2.4-My pacing of glacial–interglacial asymmetry and is associated with lower atmospheric CO_2 levels (Fig. 3) (6, 7). Asymmetry in the data series is particularly pronounced during 405-ky Eccentricity Cycles 57 and 49 (at ~22.7 and 19.5 My ago), which are characterized by distinctly sawtooth-shaped ~110-ky cycles, suggesting a causal link between cycle amplitude and asymmetry during the Early Miocene, but not during the MOGI. The distinctly asymmetric cycles suggest that the Early Miocene Antarctic ice sheets periodically underwent intervals of growth that were prolonged relative to astronomical forcing and then underwent subsequent rapid retreat in a manner akin to the glacial terminations of the Late Pleistocene glaciations, in which the large ice sheets of the Northern Hemisphere were major participants (27, 28, 32). The highly asymmetric (sawtooth) nature of Late Pleistocene glacial–interglacial cycles is thought to originate from a positive ice mass balance that persists through several precession- and obliquity-paced summer insolation maxima. This results in decreasing ice sheet stability and more rapid terminations every ~110 ky, once the ablation of the Northern Hemisphere ice sheets increases dramatically in response to the next insolation maximum. The increase in ablation is caused by lowered surface elevation of the ice sheets resulting from crustal sinking and delayed isostatic rebound (33). Similar mechanisms are implied for the large Antarctic ice sheets of the OMT (~22.5 My ago) but it is less clear why the smaller ice sheets of the Early Miocene (~19.5 My ago) would exhibit this distinctly sawtooth-shaped pattern of growth and decay (Fig. 3).

Climate–Cryosphere Evolution

Analysis of the new $\delta^{18}O$ record from Site 1264 raises two important questions: (*i*) Why did Antarctic ice sheets decrease in size after the OMT? (*ii*) Why was hysteresis (i.e., glacial–interglacial asymmetry) apparently stronger for both the large OMT and the smaller Early Miocene ice sheets than for the large ice sheets of the Oligocene? One explanation for the long-term change in ice volume is that the large glacial ice volumes of the MOGI were possible because of higher topography in West Antarctica (34) that permitted formation of a large terrestrial ice sheet that also buttressed growth of ice sheets on East Antarctica (25, 35). In this interpretation, tectonic subsidence and glacial erosion during the Late Oligocene caused a shift to a smaller marine-based ice sheet in West Antarctica (25, 35), which limited the maximum size of the Early Miocene Antarctic ice sheets during peak glacial intervals.

The Early Miocene ice sheets may have been less responsive to astronomically paced changes in radiative forcing because of colder polar temperatures under lower CO_2 conditions from ~24 My ago onward (7) or restriction of ice sheets to regions of East Antarctica above sea level following the Late Oligocene subsidence of West Antarctica (25, 35). Another possibility is that

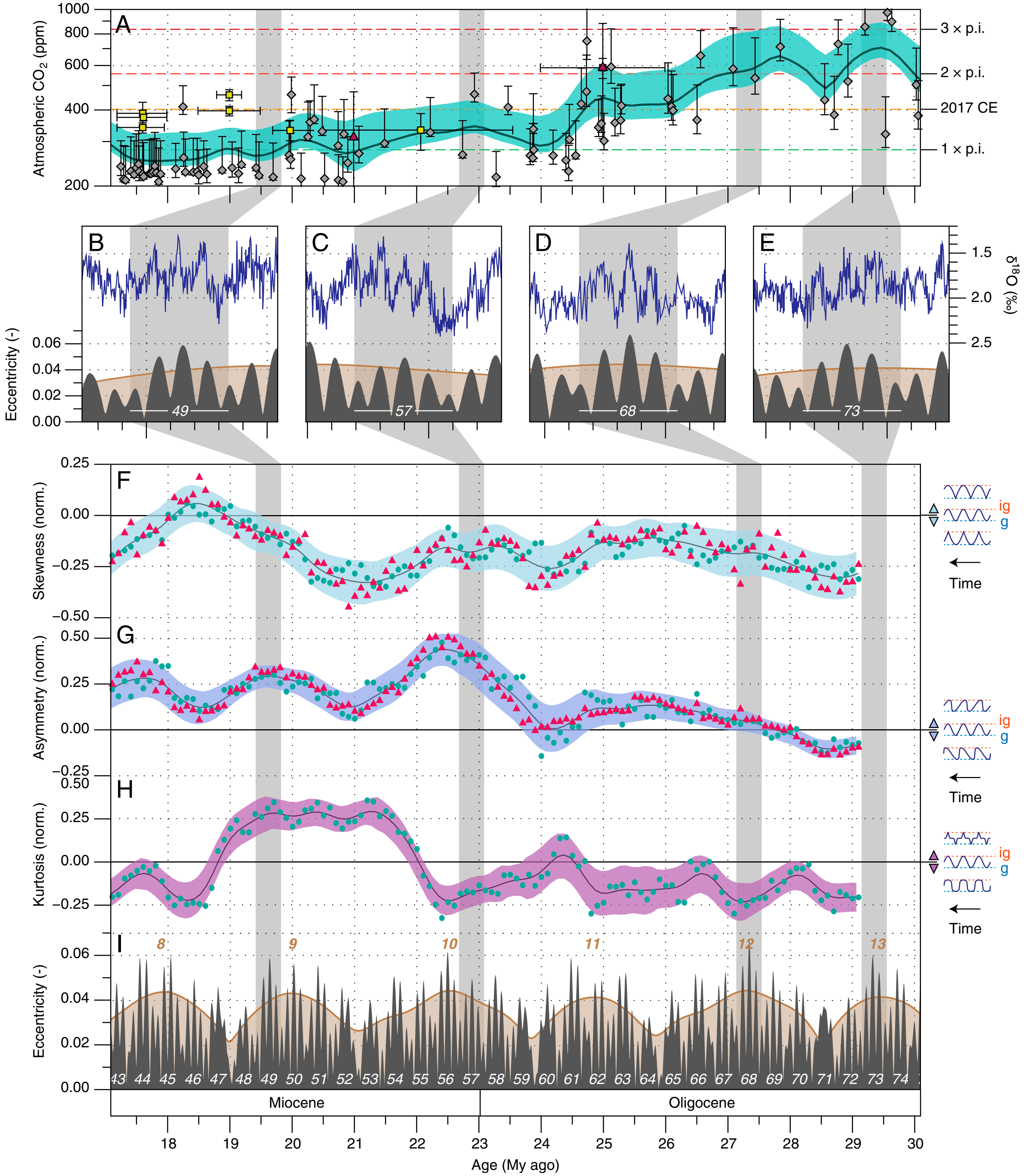

Fig. 3. Nonsinusoidal glacial–interglacial cycle properties. (*A*) Atmospheric CO_2 proxy estimates for the Oligo-Miocene and their long-term smooths (turquoise line and area; see *SI Methods*) through the reconstructed values and their maximum and minimum error estimates (black error bars). Gray diamonds represent phytoplankton CO_2 estimates, yellow squares are based on stomata, and purple-red triangles represent CO_2 estimates based on paleosols (6, 7). Multiplication factors on the right refer to preindustrial (p.i.) CO_2 concentrations of 278 ppm. CE, Common Era. (*B*–*E*) Four 405-ky-long intervals with exceptionally strong ~110-ky cycles in benthic $\delta^{18}O$, plotted against eccentricity and its ~2.4-My component (+0.02 to aid visibility). These intervals occur during (*B*) the Early Miocene, contemporaneous with 405-ky Eccentricity Cycle 49; (*C*) the Oligo-Miocene transition, Cycle 57; (*D*) the mid-Oligocene, Cycle 68; and (*E*) the Early Oligocene, Cycle 73 (white italic numbers). For *B*–*E* only, long ticks on the age axis indicate 500-ky steps, and short ticks indicate 100-ky steps. (*F*–*H*) Nonsinusoidal glacial–interglacial cycle properties. (*F*) Skewness, (*G*) asymmetry, and (*H*) kurtosis of the Site 1264 benthic $\delta^{18}O$ record quantified over a 2-My-long sliding window using standard (turquoise circles) and bispectral (purple-pink triangles) methods (see *SI Methods*). The colored areas indicate the 2σ upper and lower ranges of the cycle geometries. (*I*) Earth's orbital eccentricity (8) and its ~2.4-My component (+0.02 to aid visibility) marked by brown bold italic cycle numbers. Vertical gray bars are as in Fig. 1. To the right of *F*–*H*, the corresponding cycle shapes are depicted, and the direction of time is indicated; ig, interglacial; g, glacial.

the large ice sheets that characterized the peak glacials of the MOGI underwent rapid major growth and decay because of higher-amplitude glacial–interglacial CO_2 changes than during the Early Miocene. Such hypothesized high-amplitude changes in CO_2 would have had a direct effect on radiative forcing, which, in turn, would have caused faster feedbacks and a more linear response to eccentricity modulation of precession. Given that larger ice volumes are to be expected in a climatic state that is characterized by high cycle asymmetry and low atmospheric CO_2 concentration, a third possibility is that the conservative calculations substantially underestimate true ice volumes for the Early Miocene. Each of these hypotheses can be tested through a combination of scientific drilling on the West Antarctic shelf margin and development of high-resolution CO_2 and marine temperature proxy records with astronomical age control. We predict that strong eccentricity-driven CO_2 cycles (~110, 405, and ~2,400 ky) that are closely in step with ice volume changes will emerge in proxy CO_2 reconstructions for the Oligo-Miocene time interval. Assuming that changes in partitioning of the benthic $\delta^{18}O$ signal between temperature and ice volume are modest throughout the Oligo-Miocene, the deep-sea $\delta^{18}O$ record from Site 1264 suggests a clear long-term shift from a more glacial Oligocene to a less glacial Early Miocene climate state—a pattern of change not readily reconciled with the long-term decrease in published CO_2 records.

ACKNOWLEDGMENTS. We thank David Heslop and Lie-Liang Yang for insightful discussions and assistance. We are greatly indebted to the scientists and supporting staff of Ocean Drilling Program (ODP) Leg 208. We used samples provided by ODP, sponsored by the US National Science Foundation and participating countries under the management of the Joint Oceanographic Institutions. This research was made possible by European Research Council Grants 215458 (GTS-NEXT, to F.J.H.) and 617462 (EARTHSEQUENCING, to H.P.); Nederlandse organisatie voor Wetenschappelijk Onderzoek (NWO) Grants 864.02.007 (to L.J.L.), 865.10.001 (to L.J.L.), and 821.01.012 (to G.R.); Natural Environment Research Council (NERC) Grant NE/K014137/1 (to P.A.W.); and a Royal Society Wolfson award (to P.A.W.).

1. Zachos JC, Dickens GR, Zeebe RE (2008) An early Cenozoic perspective on greenhouse warming and carbon-cycle dynamics. *Nature* 451(7176):279–283.
2. Zachos JC, Breza JR, Wise SW (1992) Early Oligocene ice-sheet expansion on Antarctica: Stable isotope and sedimentological evidence from Kerguelen Plateau, southern Indian Ocean. *Geology* 20:569–573.
3. Coxall HK, Wilson PA, Pälike H, Lear CH, Backman J (2005) Rapid stepwise onset of Antarctic glaciation and deeper calcite compensation in the Pacific Ocean. *Nature* 433(7021):53–57.
4. Naish TR, et al. (2001) Orbitally induced oscillations in the East Antarctic ice sheet at the Oligocene/Miocene boundary. *Nature* 413(6857):719–723.
5. Bailey I, et al. (2013) An alternative suggestion for the Pliocene onset of major northern hemisphere glaciation based on the geochemical provenance of North Atlantic Ocean ice-rafted debris. *Quat Sci Rev* 75:181–194.
6. Beerling DJ, Royer DL (2011) Convergent Cenozoic CO_2 history. *Nat Geosci* 4:418–420.
7. Zhang YG, Pagani M, Liu Z, Bohaty S, DeConto R (2013) A 40-million-year history of atmospheric CO_2. *Phil Trans A Math Phys Eng Sci* 371(2001):20130096.
8. Laskar J, Gastineau M, Delisle J-B, Farrés A, Fienga A (2011) Strong chaos induced by close encounters with Ceres and Vesta. *Astron Astrophys* 532(L4):1–4.
9. Pälike H, et al. (2006) The heartbeat of the Oligocene climate system. *Science* 314(5807):1894–1898.
10. Wade BS, Pälike H (2004) Oligocene climate dynamics. *Paleoceanography* 19::PA4019.
11. Holbourn A, Kuhnt W, Kochhann KGD, Andersen N, Meier KJS (2015) Global perturbation of the carbon cycle at the onset of the Miocene Climatic Optimum. *Geology* 48(2):123–126.
12. Liebrand D, et al. (2011) Antarctic ice sheet and oceanographic response to eccentricity forcing during the early Miocene. *Clim Past* 7:869–880.
13. Zachos JC, Shackleton NJ, Revenaugh JS, Pälike H, Flower BP (2001) Climate response to orbital forcing across the Oligocene-Miocene boundary. *Science* 292(5515):274–278.
14. Zachos JC, et al. (2004) *Initial Reports: Leg 208*. Proceedings of the Ocean Drilling Program (US Gov Print Off, Washington, DC), Vol 208.
15. Liebrand D, et al. (2016) Cyclostratigraphy and eccentricity tuning of the early Oligocene through early Miocene (30.1–17.1 Ma): *Cibicides mundulus* stable oxygen and carbon isotope records from Walvis Ridge Site 1264. *Earth Planet Sci Lett* 450:392–405.
16. DeConto RM, et al. (2008) Thresholds for Cenozoic bipolar glaciation. *Nature* 455(7213):652–656.
17. Miller KG, et al. (2005) The Phanerozoic record of global sea-level change. *Science* 310(5752):1293–1298.
18. De Boer B, Van de Wal RSW, Bintanja R, Lourens LJ, Tuenter E (2010) Cenozoic global ice-volume and temperature simulations with 1-D ice-sheet models forced by benthic $\delta^{18}O$ records. *Ann Glaciol* 51(55):23–33.
19. Pälike H, Frazier J, Zachos JC (2006) Extended orbitally forced palaeoclimatic records from the equatorial Atlantic Ceara Rise. *Quat Sci Rev* 25(23-24):3138–3149.
20. Beddow HM, Liebrand D, Sluijs A, Wade BS, Lourens LJ (2016) Global change across the Oligocene-Miocene Transition: High-resolution stable isotope records from IODP Site U1334 (equatorial Pacific Ocean). *Paleoceanography* 31:81–97.
21. Valero L, Cabrera L, Sáez A, Garcés M (2016) Long-period astronomically-forced terrestrial carbon sinks. *Earth Planet Sci Lett* 444:131–138.
22. Valero L, Garcés M, Cabrera L, Costa E, Sáez A (2014) 20 Myr of eccentricity paced lacustrine cycles in the Cenozoic Ebro Basin. *Earth Planet Sci Lett* 408:183–193.
23. van Dam JA, et al. (2006) Long-period astronomical forcing of mammal turnover. *Nature* 443(7112):687–691.
24. Elderfield H, et al. (2012) Evolution of ocean temperature and ice volume through the mid-Pleistocene climate transition. *Science* 337(6095):704–709.
25. Gasson E, DeConto RM, Pollard D, Levy RH (2016) Dynamic Antarctic ice sheet during the early to mid-Miocene. *Proc Natl Acad Sci USA* 113(13):3459–3464.
26. Hasselmann K, Munk W, MacDonald G (1963) Bispectra of ocean waves. *Proceedings of the Symposium on Time Series Analysis*, ed Rosenblatt M (Wiley, New York), pp 125–139.
27. Hagelberg T, Pisias N, Elgar S (1991) Linear and nonlinear couplings between orbital forcing and the marine $\delta^{18}O$ record during the late Neogene. *Paleoceanography* 6(6):729–746.
28. King T (1996) Quantifying nonlinearity and geometry in time series of climate. *Quat Sci Rev* 15:247–266.
29. DeConto RM, Pollard D (2016) Contribution of Antarctica to past and future sea-level rise. *Nature* 531(7596):591–597.
30. Mawbey EM, Lear CH (2013) Carbon cycle feedbacks during the Oligocene-Miocene transient glaciation. *Geology* 41(9):963–966.
31. DeConto R, Pollard D, Harwood D (2007) Sea ice feedback and Cenozoic evolution of Antarctic climate and ice sheets. *Paleoceanography* 22:PA3214.
32. Lisiecki LE, Raymo ME (2007) Plio-Pleistocene climate evolution: Trends and transitions in glacial cycle dynamics. *Quat Sci Rev* 26(1-2):56–69.
33. Abe-Ouchi A, et al. (2013) Insolation-driven 100,000-year glacial cycles and hysteresis of ice-sheet volume. *Nature* 500(7461):190–193.
34. Fretwell P, et al. (2013) Bedmap2: Improved ice bed, surface and thickness datasets for Antarctica. *Cryosphere* 7(1):375–393.
35. Levy R, et al.; SMS Science Team (2016) Antarctic ice sheet sensitivity to atmospheric CO_2 variations in the early to mid-Miocene. *Proc Natl Acad Sci USA* 113(13):3453–3458.
36. Miller KG, Fairbanks RG, Mountain GS (1987) Tertiary oxygen isotope synthesis, sea level history, and continental margin erosion. *Paleoceanography* 2(1):1–19.
37. Marchitto TM, et al. (2014) Improved oxygen isotope temperature calibrations for cosmopolitan benthic foraminifera. *Geochim Cosmochim Acta* 130:1–11.
38. Schlitzer R (2010) Ocean Data View 4, version 4.3.6. Available at odv.awi.de. Accessed November 2010.
39. Bohaty SM, Zachos JC, Delaney ML (2012) Foraminiferal Mg/Ca evidence for Southern Ocean cooling across the Eocene–Oligocene transition. *Earth Planet Sci Lett* 317-318:251–261.
40. Petersen SV, Schrag DP (2015) Antarctic ice growth before and after the Eocene-Oligocene transition: New estimates from clumped isotope paleothermometry. *Paleoceanography* 30:1305–1317.
41. Bamber JL, Layberry RL, Gogineni S (2001) A new ice thickness and bed data set for the Greenland ice sheet 1. Measurement, data reduction, and errors. *J Geophys Res Atmos* 106(D24):33773–33780.
42. Charette MA, Smith WHF (2010) The volume of Earth's ocean. *Oceanography (Wash DC)* 23(2):112–114.
43. Paillard D, Labeyrie L, Yiou P (1996) AnalySeries, Macintosh program performs time-series analysis. *Eos Trans AGU* 77(39):379.
44. Beddow HM, et al. (2016) Early to middle Miocene climate evolution: Benthic oxygen and carbon isotope records from Walvis Ridge Site 1264. *Orbital forcing and climate response; astronomically-tuned age models and stable isotope records for the Oligocene-Miocene*, ed Beddow HM (Utrecht Univ, Utrecht, The Netherlands), Vol PhD.
45. Chaudhuri P, Marron JS (1999) SiZer for exploration of structures in curves. *J Am Stat Assoc* 94(447):807–823.
46. Herbers THC, Russnogle NR, Elgar S (2000) Spectral energy balance of breaking waves within the surf zone. *J Phys Oceanogr* 30:2723–2737.
47. Elgar S (1987) Relationships involving third moments and bispectra of a harmonic process. *IEEE Trans Acoust Speech Signal Process* 35(12):1725–1726.
48. De Bakker ATM, Herbers THC, Smit PB, Tissier MFS, Ruessink BG (2015) Nonlinear infragravity-wave interactions on a gently sloping laboratory beach. *J Phys Oceanogr* 45:589–605.
49. Doering JC, Bowen AJ (1995) Parametrization of orbital velocity asymmetries of shoaling and breaking waves using bispectral analysis. *Coast Eng* 26:15–33.
50. Kennedy AB, Chen Q, Kirby JT, Dalrymple RA (2000) Boussinesq modeling of wave transformation, breaking, and runup. I: 1D. *J Waterw Port Coast Ocean Eng* 126:39–47.
51. Pearson K (1905) Skew variation, a rejoinder. *Biometrika* 4:169–212.
52. Herbert TD (1994) Reading orbital signals distorted by sedimentation: Models and examples. *Spec Publ Int Assoc Sedimentol* 19:483–507.
53. Bard E (2001) Paleoceanographic implications of the difference in deep-sea sediment mixing between large and fine particles. *Paleoceanography* 16(2):235–239.
54. Lisiecki LE, Raymo ME (2005) A Pliocene-Pleistocene stack of 57 globally distributed benthic $\delta^{18}O$ records. *Paleoceanography* 20:PA1003.